JACS
JOURNAL OF THE AMERICAN CHEMICAL SOCIETY

Article

pubs.acs.org/JACS

Scalable Bromide-Triggered Synthesis of Pd@Pt Core–Shell Ultrathin Nanowires with Enhanced Electrocatalytic Performance toward Oxygen Reduction Reaction

Hui-Hui Li, Si-Yue Ma, Qi-Qi Fu, Xiao-Jing Liu, Liang Wu, and Shu-Hong Yu*

Division of Nanomaterials and Chemistry, Hefei National Laboratory for Physical Sciences at Microscale, Collaborative Innovation Center of Suzhou Nano Science and Technology, Department of Chemistry, University of Science and Technology of China, Hefei, Anhui 230026, The People's Republic of China

Supporting Information

ABSTRACT: This article reports a novel scalable method to prepare ultrathin and uniform Pd@Pt nanowires (NWs) with controllable composition and shell thickness, high aspect ratio, and smooth surface, triggered by bromide ions via a galvanic replacement reaction between $PtCl_6^{2-}$ and Pd NWs. It was found that bromide ions played a vital role in initiating and promoting the galvanic reaction. The bromide ions served as capping and oxidized etching agents, counterbalancing the Pt deposition and Pd etching on the surface to give final Pd@Pt core–shell nanostructures. Such a counterbalance and the formation $PtBr_6^{2-}$ with lower redox potential could lower the reaction rate and be responsible for full coverage of a smooth Pt shell. The full coverage of Pt deposited on Pd NWs is important for the enhancement of the activity and stability, which depend strongly on the Pt content and Pt shell thickness. Significantly, the Pd@Pt NWs with Pt content of 21.2% (atomic ratio) exhibited the highest mass activity (810 mA mg^{-1}_{Pt}) and specific activity (0.4 mA cm^{-2}). Interestingly, the mass activity (1560 mA mg^{-1}_{Pt}) and specific activity (0.98 mA cm^{-2}) of Pd@Pt (21.2%) NWs increased to 2.45 and 1.95 times the initial values after 60k cycles tests, 8.5 and 9.0 times greater than those of Pt/C catalysts. In addition, these ultrathin NW electrocatalysts with large aspect ratio are easy to form into a freestanding film, which improves the mass transport, electrical conductivity, and structure stability.

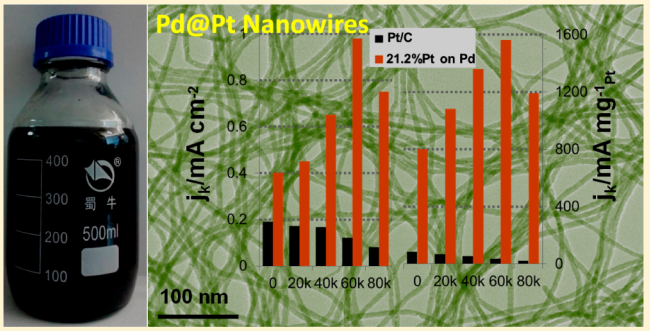

INTRODUCTION

Over the past decades, extensive research has been devoted to electrocatalysis studies to improve the performance of catalysts with high activity and low material loading to meet the cost requirement for practical use by the general public.[1] High cost, poor durability, and sluggish kinetics predominantly hindered the commercialization of fuel cells for pure Pt catalysts.[2] One promising strategy involves the design and synthesis of Pt-based and non-noble-metal catalysts with low Pt loading and low cost to meet the challenges for fuel cell application.[3] Among these catalysts, Pt-based core–shell or core–shell-like structures combine the advantages of Pt and non-noble metals and exhibit excellent activity with low Pt content, because only the surface or sub-surface of the catalyst is needed to work in electrocatalysis.[4] Ultrathin or monolayer Pt-rich shells supported on other metal cores could considerably reduce the Pt usage and optimize the reactivity through the interaction between the shell and the core, such as ligand effect and strain effect.[5] At the anode, bilayer Ru@Pt core–shell electrocatalysts exhibited both enhanced corrosion resistance and CO tolerance.[6] At the cathode, Pt monolayer on PdAu nanoparticles (NPs) or Pd@$Pt_{1.8}$Ni core–shell nanocrystals, or Pt shell on ordered PtCo intermetallic core NPs, exhibited excellent activity and stability for the oxygen reduction reaction (ORR).[7] In this regard, the design and synthesis of multicomponent core–shell structure materials play important roles in developing novel electrolcatalysts and achieving superior catalytic performance.

Until now, many synthetic methods to generate core–shell structure have been studied. Adzic's group prepared series of nanoscale core–shell structures with a Pt monolayer supported on single-crystal substrates, Pd/C, PdAu, IrNi, and $AuNi_{0.5}Fe$, via the galvanic replacement of an under-potentially deposited (UPD) Cu monolayer.[7a,8] This is an effective and controlled method to fabricate one-atomic-layer Pt electrocatalysts with ultralow Pt content and high Pt utilization, improved by the modification of the top layer of the core materials. Scale-up for production may be the limitation of this method, due to the confined electrode area. A seed-mediated method has been widely used to grow a Pt or Pt alloy shell on non-noble-metal cores but usually needs surfactants to control the size and shape of the final products.[9] Sun and co-workers recently reported the synthesis of FeNiPt/Pt core–shell nanowires (NWs) in the

Received: April 14, 2015
Published: May 26, 2015

DOI: 10.1021/jacs.5b03877
J. Am. Chem. Soc. 2015, 137, 7862–7868

presence of oleylamine and oleic acid at high temperatures, combining acid etching and thermal annealing processes. A Pt-skeleton or Pt-skin core−shell structure was obtained, showing higher activity and better stability comparing with FeNiPt core NWs and Pt NPs.[10] A wide range of materials, such as Pt overlayers on tungsten carbide, anodic aluminum oxide membranes, Pd metal, and so on, have been fabricated by atomic layer deposition (ALD), which is able to control the thickness of the layers with atomic-level precision due to the slow chemisorption kinetics of the metal precursors. Layer-by-layer growth of the core−shell catalyst by ALD has some merits, but this method wastes much of the noble-metal precursor and has a lower usage efficiency.[11] Another usual protocol to prepare core−shell structure is the chemical reduction method, using ascorbic acid (AA), citric acid (CA), and $NaBH_4$ as reductants. The reduction rate can be controlled by the capacity of reducing agent. Xia's group systematically evaluated the electrochemical performance of octahedral Pd@Pt_{nL} core−shell catalysts, prepared by two different approaches using AA and CA as reducing agent, respectively. The octahedral Pd@Pt_{nL} core−shell catalysts exhibited 4-fold enhancement in specific activity for the ORR compared with commercial Pt/C.[12] Wang and co-workers demonstrated a wet-chemical strategy to synthesize Pt/Pd bimetallic nanotubes with petal-like surfaces decorated with a Pd shell using AA as reducing agent, exhibiting enhanced activity and stability toward ethanol electrooxidation.[13] The as-prepared catalyst coupling with surface segregation and dealloying also is an efficient way to produce Pt-rich shell catalysts, affecting the catalytic performance.[14] However, although a range of techniques have been developed to produce core−shell nanostructures with multicomposition and mainly with zero-dimension structure, the construction of core−shell structures based on one dimension (self-supported electrode) with deposited smooth surface and ultrafine size by a facile strategy and scale-up remains a challenge.

Here, we demonstrate a novel method to prepare ultrathin and uniform Pd@Pt NWs with controllable composition, controllable shell thickness, high aspect ratio, and smooth surface, induced by bromide ions via a galvanic replacement reaction. Ultrathin, ultralong, and high-quality Te NWs were used as partial sacrificial templates to obtain PdTe NWs, and then Pd NWs were obtained by oxidized etching PdTe NWs. The bromide ions play an important role in initiating and promoting the galvanic reaction. Meanwhile, bromide ions as both capping and oxidized etching agents counterbalance the Pt deposition and Pd etching on the surface with a lower reaction rate, giving a final Pd@Pt core−shell structure with smooth surface. This method is easy to scale up due to the mass production of Te NWs (1.6 L for one time) and the mild reaction conditions. The electrochemical performance of Pd@Pt NWs is strongly dependent on the Pt content and shell thickness, which can be tuned by the use of Pt precursors. Pd@Pt NWs with Pt content of 21.2% (atomic ratio) exhibited the highest activity and best stability.

EXPERIMENTAL SECTION

Chemicals. Na_2TeO_3, poly(vinylpyrrolidone) (PVP, degree of polymerization (DP) = 360), H_2PtCl_6, hydrazine hydrate (85% w/w %), HCl, aqueous ammonia solution (25−28% w/w%), ethanol, and isopropyl alcohol were purchased from Shanghai Chemical Reagent Co. Ltd., Nafion (5 wt%) from Sigma-Aldrich, and $PdCl_2$ from J&K Chemical Ltd. All the chemical reagents were used as received without further purification. Doubly distilled deionized water (DIW, 18.2 MΩ) was used for all preparations in the synthesis of ultrathin Te NWs and Pd-based NWs.

Large-Scale Synthesis of Ultrathin Te NWs. A procedure developed by our group recently was used to prepare the high quality Te NWs in large scale.[15] Briefly, we added PVP (10.0 g) and Na_2TeO_3 (4.0 mmol) into 350 mL of DIW under magnetic stirring at room temperature, and then added hydrazine hydrate (17 mL) and aqueous ammonia solution (33 mL). The mixture was transferred to a Teflon vessel held in a stainless steel autoclave (500 mL), heating at 180 °C for 3 h.

Large-Scale Synthesis of Ultrathin Pd NWs. Acetone was added into the as-prepared solution of Te NWs described above, which was collected by strong shaking to separate Te NWs from the solution and then dispersed into 100 mL of DIW. Next, PdTe NWs were prepared by adding 90 mL of H_2PdCl_4 (25 mM $PdCl_2$ dissolved into HCl with mole ratio of 1:2 to obtain H_2PdCl_4 solution) aqueous solution into the Te NWs aqueous solution under magnetic stirring at room temperature for 5 h. The PdTe NWs were collected in the same way as the Te NWs, and then these PdTe NWs were dispersed into 0.01 M NaOH solution with vigorous magnetic stirring for 3 h to remove Te atoms, giving Pd NWs. Finally, the products were washed several times with DIW and dispersed into 100 mL of water.

Scalable Synthesis of Ultrathin Pd@Pt Core−Shell NWs. In a typical procedure, 8 μmol of the aqueous suspension of Pd NWs and 15 mL of an aqueous solution containing KBr (300 mg) were mixed in a glass vial. The mixture was stirred for 15 min. Next, 0.1 mL of H_2PtCl_6 (40 mM) aqueous solution was added dropwise to the aboveaqueous solution under magnetic stirring at room temperature. The reaction was taken at a rotation rate of 260 rpm using an Innova 40 benchtop incubator shaker for 3 h at 80 °C. The products were collected by centrifuging (10 000 rpm, 5 min) and then washed with ethanol three times. We systematically investigated the effects of various parameters, including the reaction time, the reaction temperature, the amount of H_2PtCl_6, and the amount of KBr as well as KCl and KI, on the composition and shell thickness of the resultant Pd@Pt NWs. We were successful in scaling up production by 300 times compared to the typical procedure (a 10 times increase for the precursors) to prepare the Pd@Pt core−shell NWs (limited by the height of the shaker).

Electrochemical Measurements. A three-electrode system containing a rotating disk electrode (RDE, Pine Research Instrumentation, United States) connected to a potentiostat (Metrohm Autolab, Switzerland) at room temperature was used for electrochemical measurments. The counter and reference electrodes were a platinum foil and Ag/AgCl (3.5 M), respectively. Ethanol suspensions of the Pd and Pd@Pt catalysts were dropped on the surface of pre-polished and cleaned RDEs (5 mm diameter, 0.196 cm^2) and then covered with 10 μL of 0.02 wt% Nafion (diluted from 5 wt% Nafion, Sigma-Aldrich). Finally, the electrode was dried in flowing argon. For comparison, 5 mg Pt/C catalysts (20 wt%, Johnson Matthey) were added into the mixture of 5 mL of isopropyl alcohol and 25 μL of 5 wt% Nafion before 30 min of ultrasonication. Cyclic voltammetry (CV) was carried out in an Ar-saturated 0.1 M $HClO_4$ solution at 50 mV s^{-1} at room temperature. The ORR measurements and durability testing were carried out in O_2-saturated 0.1 M $HClO_4$ solution at 5 mV s^{-1} and at a rotation rate of 1600 rpm. During the durability testing, the electrode was cycled from 0.5 to 1.1 V for 80k cycles and was left open to the atmosphere. The electrochemically active surface area (ECSA) and polarization curves for the ORR were measured after every 10k cycles. The Pt/C catalysts were measured under the same conditions with Pd@Pt NWs. All potentials reported in this paper were normalized with respect to the reversible hydrogen electrode (RHE).

Instruments. X-ray powder diffraction (XRD) patterns were obtained using a Rigaku (Japan) DMax-γA rotation anode X-ray diffractometer equipped for graphite-monochromatized Cu K radiation (λ = 1.54178 Å). Transmission electron microscopy (TEM), high-resolution TEM (HRTEM), and high-angle annular dark-field scanning TEM (HAADF-STEM) were performed using Hitachi H-

DOI: 10.1021/jacs.5b03877
J. Am. Chem. Soc. 2015, 137, 7862−7868

7650 and JEM-ARM 200F atomic-resolution analytical microscopes operating at an accelerating voltage of 200 kV. Elemental mappings were done using a Gatan GIF Quantum 965 instrument. Energy-dispersive spectrometry (EDS) and scanning transmission electron microscopy–energy dispersive spectrometry (STEM-EDS) element mapping were carried out on a JEOL-2010F transmission electron microscope equipped with an Oxford INCA system. Electrochemical measurements were performed on a potentiostat (Metrohm Autolab, Switzerland).

RESULTS AND DISCUSSION

Formation of Core–Shell Nanostructures. We monitored the evolution of Pd@Pt ultrathin NWs with different compositions and Pt shell thicknesses during galvanic replacement reactions. The high-quality ultrathin Te NWs were prepared on a large scale by the method we developed previously.[16] First, we prepared PdTe NWs using Te NWs as partial templates through a galvanic replacement to avoid adding excessive Pd precursors and lower the cost.[17] It is a modified method based on our previous work: the excess of Pd precursors is twice of that of Te NWs to obtain Pd NWs.[18] These PdTe NWs were then dispersed into oxygen-saturated 0.01 M NaOH solution to remove Te atoms and obtain Pd NWs. Figure S1 shows the TEM images of uniform PdTe and Pd NWs with ultrathin size. In the following experiments, Pd NWs with ultrathin size were employed as templates to prepare Pd@Pt core–shell NWs in the presence of KBr and H_2PtCl_6. It is easy to control the extent of galvanic replacement between Pd NWs and $PtCl_6^{2-}$ ions by varying a set of experimental parameters, such as the amount of H_2PtCl_6, reaction temperature, the amount of KBr, and reaction time.

Figures 1A and 2 show typical TEM images of uniform Pd@Pt NWs that were prepared using the typical procedure with

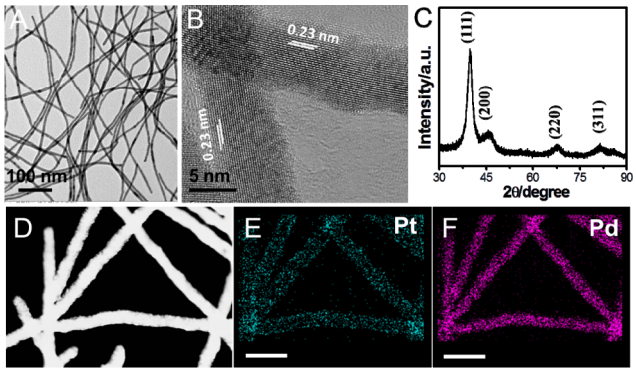

Figure 1. TEM image (A), HRTEM image (B), and XRD pattern (C) of the Pd@Pt (21.2%) NWs prepared by the typical procedure. HAADF/STEM image (D) and EDS mapping analysis showing the elements Pt (E) and Pd (F) dispersed on the Pd@Pt (21.2%) NWs uniformly. Scale bar, 20 nm.

different amounts of H_2PtCl_6. TEM images confirm that all the Pd@Pt NWs display good uniformity in terms of the morphology and ultrathin size (7–9 nm). The HRTEM image and XRD pattern in Figure 1B,C clearly show typical (111) lattice fringes and corresponding fcc diffraction peaks for a Pt shell with a Pd core. Such one-dimensional (1D) Pd@Pt NWs with a high ratio of Pt atoms on (111) planes could enhance the electrocatalytic performance due to less low-coordination sites and edges.[19] As shown in Figure 5 (below), the plot of the variation of Pt atomic ratio with the addition of H_2PtCl_6 based on the inductively coupled plasma mass

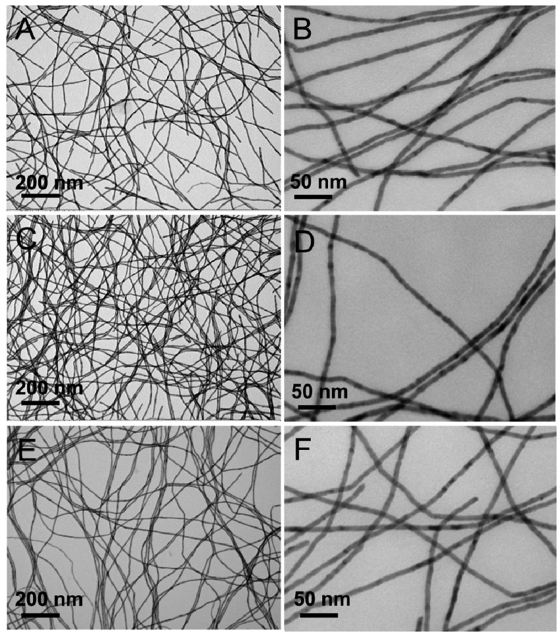

Figure 2. TEM images of Pd@Pt NWs with Pt atomic ratios of 6.0% (A,B), 13.5% (C,D), and 28.5% (E,F), prepared using the typical procedure with different amounts of H_2PtCl_6.

spectroscopy (ICPMS) data indicates that the Pt content increased with increasing amount of H_2PtCl_6. Pt atomic ratios of 6.0%, 13.5%, 21.2%, and 28.5% are obtained (Figure 5A) by controlling the amount of H_2PtCl_6 added into the reaction as well as the different Pt-rich shell thicknesses (Figure 3).

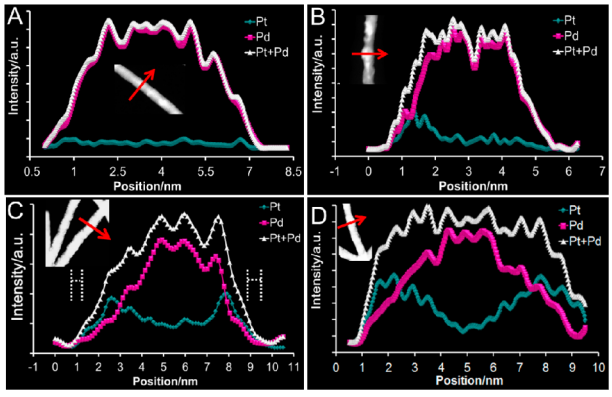

Figure 3. Distribution of the components in the Pd@Pt (6.0%) (A), Pd@Pt (13.5%) (B), Pd@Pt (21.2%) (C), and Pd@Pt (28.5%) NWs (D) obtained by the line-scan analysis using STEM-EDS (along the red arrow in the inset). The shell thickness of Pd@Pt (21.2%) NWs was 0.5–0.8 nm, as shown by the dashed line.

The core–shell structure and component distribution of Pd@Pt NWs are confirmed by the HADDF-STEM images in the inset and the line-profile analysis using STEM-EDS. As shown in Figure 3, there is a clear contrast in the HADDF-STEM images in the inset between Pt and Pd, because Pt (Z = 78) has a much higher atomic number than Pd (Z = 46). The bright area was assigned to Pt, which surrounds the darker Pd core. For Pd@Pt (6.0%) and Pd@Pt (13.5%) NWs, the Pd core NWs were not covered fully by the Pt shell, leaving many Pd atoms exposed. However, there is a bright area (Pt layer) that can be seen for Pd@Pt (21.2%) and Pd@Pt (28.5%) NWs

DOI: 10.1021/jacs.5b03877
J. Am. Chem. Soc. 2015, 137, 7862–7868

with higher Pt content, indicating the formation of a core−shell structure with full coverage of a Pt shell on the Pd core NWs. Figure 3 shows the intensity profiles in a line scan across a Pd@Pt NW, further verifying the formation of a Pt shell and determining the Pt shell thickness. As shown in Figure 3C, we estimate the Pt shell thickness of Pd@Pt (21.2%) NWs to be 0.5−0.8 nm, corresponding to three or more Pt-rich layers, which is thinner than that of Pd@Pt (28.5%) NWs.[20] Such a Pt-rich shell thickness may lead to a negligible ligand effect, but it also may induce a compressive strain in the surface metal.[5a] The superposition of Pt and Pd signals at the position of 7−8 nm can be assigned to the boundaries between Pt and Pd elements, indicating partial PtPd alloying at the interface. Figure 1D−F shows the HADDF-STEM image and the corresponding elemental mapping of Pd@Pt (21.2%) NWs, indicating that the component is distributed uniformly along the NWs. We can conclude that the Pt concentration and the Pt shell thickness could be easily controlled by tuning the amount of H_2PtCl_6 and that both values are proportional.

As shown in Figure 4, we also prepared Pd@Pt core−shell NWs successfully on a large scale by magnifying the typical

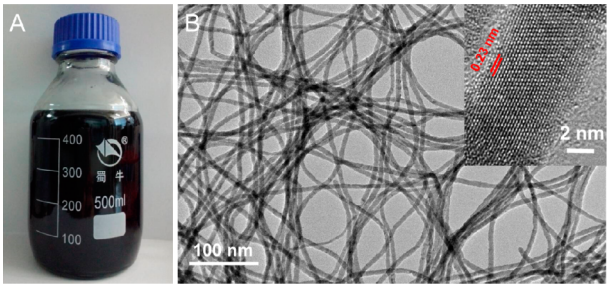

Figure 4. (A) Photograph of the scaled-up synthesized Pd@Pt NWs dispersed in ethanol. (B) TEM and HRTEM (inset) images of the Pd@Pt NWs with uniform and ultrathin size, which are similar to those of the Pd@Pt NWs prepared by the typical procedure.

production procedure by 300 times (limited by the height of the shaker). The good dispersion of the reaction system and controlled kinetics ensure its scalability. The large-scale synthesized Pd@Pt NWs have Pt content (20.8%), morphology, and core−shell structure similar to those of the Pd@Pt (21.2%) NWs prepared by the typical procedure, proving that this is a scalable method and presenting a possibility for commercialization of these NWs as cheaper electrocatalysts compared with Pt/C catalysts.

Effect of Bromide Ions on the Core−Shell Nanostructures. In the present work, we designed a series of experiments to elucidate the role of bromide ions in producing Pd@Pt ultrathin NWs. In principle, the galvanic replacement reaction between $PtCl_6^{2-}$ ions and Pd NWs can occur naturally, due to the reduction potential of $PtCl_6^{2-}$/Pt (0.74 V vs RHE) being more positive than that of $PdCl_4^{2-}$/Pd (0.62 V vs RHE). However, the reaction did not occur when no bromide ions were introduced into the reaction system. As shown in Figure S2, Pt NPs produced around the NWs may be reducing the residual PVP on the template surface; introducing bromide ions may promote the galvanic replacement reaction by changing the reduction potential, shifting the reaction equilibrium, and increasing the reaction kinetics. As shown in Figure S3, the Pd@Pt NWs were successfully prepared by the typical procedure with different amounts of KBr added into the reaction system. So, the bromide ions play a critical role in initiating and promoting the reaction for preparing Pd@Pt NWs.

When bromide ions are added, they replace chloride ions in the precursor, due to the higher stability constants for $PtBr_6^{2-}$ and $PdBr_4^{2-}$ relative to $PtCl_6^{2-}$ and $PdCl_4^{2-}$ with the same difference in redox potential values. The reaction kinetics may become slow; thus, the surface of deposited Pt shell would be smoother and the thickness easy to control. Meanwhile, the surface of Pd NWs is supposed to be capped by a layer of bromide ions when enough are added, because they are preferentially chemisorbed on the Pd surface.[21] Figure S4 shows pictures of the Pd NWs dispersion without KBr (A) and with KBr (B), shaken for 3 h at 80 °C, indicating that the Pd NWs (B) have a much better dispersion due to the capping effect of the bromide ions. The excessive bromide ions initiate and facilitate the reaction by shifting the reaction equilibrium to the side of the formation of Pt. There will be a lot of $PtBr_6^{2-}$ near the Pd NWs surface, continuing the galvanic replacement reaction.[22] As shown in Figure 5B, controlling the amount of

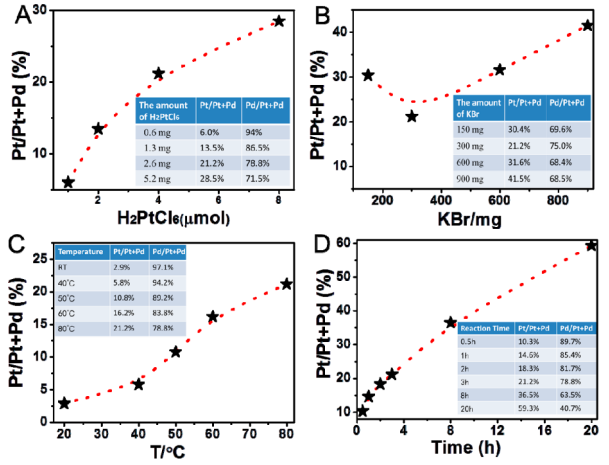

Figure 5. Changes of Pt content (atomic ratio) in Pd@Pt NWs as a function of the amount of H_2PtCl_6 (A), the amount of KBr (B), the reaction temperature (C), and the reaction time (D).

bromide ions could lead to controlling the atomic ratio of Pt to Pd. A critical amount of bromide ions may needed to cap the Pd surface and initiate the galvanic replacement reaction in order to form of a full coverage of Pt shell on the Pd surface. When a small amount of bromide ions (150 mg of KBr) was added into the reaction, the atomic ratio of Pt was 30.4%. When the amount of bromide ions was increased to 300 mg, the atomic ratio of Pt decreased to 21.2%, because more of the Pd surface was covered by bromide ions. So, the chemisorbed bromide ions may prevent the galvanic replacement reaction to some extent. Conversely, as the amount of bromide ions further increased, the atomic ratio of Pt increased. As such, the Pd NWs were preferentially etched by Br^-/O_2 in the presence of bromide ions to form $PdBr_4^{2-}$, removing some bromide ions from the surface of the Pd NWs. Together with the oxidation by $PtBr_6^{2-}$ through the galvanic replacement reaction, the atomic ratio of Pt increases, but a higher amount of KBr could decrease the total amount of the product.

To support this argument, we designed some experiments with different degrees of etching, adding different amounts of bromide ions without $PtCl_6^{2-}$. Figure S5 shows the supernatants after centrifugation of the products obtained using the typical procedure with $PtCl_6^{2-}$ (1) and without $PtCl_6^{2-}$ (2).

DOI: 10.1021/jacs.5b03877
J. Am. Chem. Soc. 2015, 137, 7862−7868

The yellow color of the supernatant in picture 1 may be due to the formation of $PtBr_6^{2-}$ and $PdBr_4^{2-}$, because $PtCl_6^{2-}$ and $PdCl_4^{2-}$ would be very light yellow and light brown, respectively, at such low concentrations. According to the ICPMS data shown in Table S1, the Pd^{2+} in the supernatant also could be generated without $PtCl_6^{2-}$, and its concentration increased as the amount of KBr increased, confirming that the Pd NWs could be oxidatively etched by Br^-/O_2. So, the bromide ions may serve multiple functions to facilitate the reaction. First, the excess bromide ions promote the reaction by shifting the reaction equilibrium. We also added the same molar concentration of chloride and iodide ions to replace bromide ions in the reaction system. Uniform and ultrathin NWs were again obtained (Figure S6), indicating that the halide ions could facilitate the galvanic replacement reaction. Second, bromide ions could serve as a capping and oxidized etching agent, counterbalancing the Pt deposition and Pd etching on the surface to obtain the final Pd@Pt core−shell structure with a smooth surface. As discussed above, slow reduction coupled with oxidative etching yields smooth and uniform Pd@Pt NWs in the presence of bromide ions.

Effects of Other Parameters. The reaction temperature, another important parameter in producing Pd@Pt NWs, can strongly influence the galvanic replacement reaction rate and the redox potential of $PtBr_6^{2-}$. As shown in Figure 5C, the atomic ratio of Pt increased with elevated temperature. Figure S7 show TEM images of Pd@Pt NWs prepared by the typical procedure with different reaction times. Although the atomic ratio of Pt is only 2.9% when the reaction is performed at room temperature, no Pt nanoparticles were generated in the presence of bromide ions. The atomic ratio of Pt increased at higher temperatures, possibly due to the accelerated reaction rate and removal of the bromide ions from the Pd surface. We believe that the higher reaction rate and corrosion of Pd are beneficial to the galvanic replacement reaction.

As shown in Figure S8, ultrathin and uniform Pd@Pt NWs were obtained by the typical procedure with different reaction times. Figure 5D shows that the atomic ratio of Pt increased as the reaction time was extended. In the typical procedure, the amount of Pt precursors added is half that of Pd. Theoretically, Pd NWs were just replaced by all the Pt precusors according to the stoichiometric ratio calculation. As the reaction proceeded, the atomic ratio of Pt increased. When the reaction time was extended to 20 h, the amount of the final products was much lower than that obtained with reaction for 3 h, due to the Pd NWs being oxidatively etched by Br^-/O_2.[21b] The extent of the galvanic replacement reaction and the atomic ratio of Pt could be easily controlled by varying the parameters.

Electrochemical Performance. Pd@Pt NWs with different Pt atomic ratios of 6.0%, 13.5%, 21.2%, and 28.5% were synthesized by a galvanic replacement reaction with different amounts of H_2PtCl_6, and then their electrochemical properties toward the ORR were studied. Figure 6A shows the CV curves for Pd@Pt NWs with different Pt atomic ratio, Pd NWs, and commercial Pt/C in Ar-saturated 0.1 M $HClO_4$ solution at a sweep rate of 50 mV s^{-1} at room temperature. The Pt coverage on the Pd core NWs can be confirmed by the CV curves. It is found that the Pd characteristic hydrogen desorption peak occurs around 0.25 V vs RHE (Figure S9, indicated by the red arrow).[23] After the Pt shell was deposited, the hydrogen desorption peak had a negative shift with increasing Pt ratio, proving the Pt deposition on Pd core NWs. The diminishment of the peak at 0.25 V vs RHE and the similar features of the

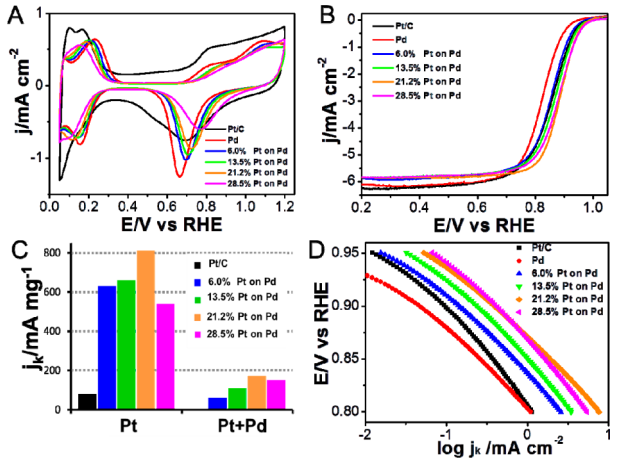

Figure 6. Electrochemical activities of Pd@Pt NWs versus Pd NWs and Pt/C. (A) CV profiles of the catalysts recorded in Ar-saturated 0.1 M $HClO_4$ solution at a sweep rate of 50 mV s^{-1}. (B) ORR polarization curves for the catalysts in O_2-saturated 0.1 M $HClO_4$ solution with a sweep rate of 5 mV s^{-1} and a rotation rate of 1600 rpm. The mass activity and specific activity are depicted as kinetic-current densities (j_k) normalized to the loading mass of the metal and the ECSA at 0.9 V (vs RHE) in (C) and (D), respectively.

Pd@Pt NWs (21.2% and 28.5%) and the Pt/C catalysts indicated the full Pt coverage on Pd NWs. The ECSA was calculated by integrating the under-potentially deposited hydrogen (H_{UPD}) adsorption/desorption charge, assuming a value of 210 μC cm^{-2}.[24] All of the samples have similar specific ECSAs with the same total noble metal loading (21.8 μg cm^{-2}).

The polarization curves for the ORR obtained with Pd@Pt NWs, Pd core NWs, and Pt/C electrocatalysts on a glassy carbon RDE in O_2-saturated 0.1 M $HClO_4$ solution at room temperature at a sweep rate of 5 mV s^{-1} are shown in Figure 6B, demonstrating that the deposition of the Pt shell and the shell thickness clearly affect the ORR activity. The Pt-based electrocatalysts containing Pd@Pt NWs and Pt/C catalyst have about 50 mV higher onset potential compared with Pd core NWs. The onset potential and half-wave potential, $E_{1/2}$, of the Pd@Pt NWs show positive shifts with increasing Pt content and Pt shell thickness. The Pd@Pt NWs (6.0%) are less active for the ORR than Pt/C catalysts, but after more Pt is deposited on Pd NWs, the Pd@Pt NWs are more active than the Pt/C catalysts. The Pd@Pt NWs with atomic ratios of 21.2% and 28.5% have similar ORR activity and show a marked positive shift in $E_{1/2}$ by ~32 mV relative to Pt/C catalysts. To better understand the intrinsic activity of the prepared electrocatalyts, the kinetic current was calculated on the basis of the ORR polarization curves and normalized to the ECSA and the amount of noble metal to obtain the mass activity and specific activity, respectively.

Figure 6C,D shows the mass activity and specific activity of Pd@Pt NWs, Pd core NWs, and Pt/C catalyst, where the Pd@Pt NWs exhibit much higher activity than Pt/C catalyst. The Pd@Pt NWs (6.0%) exhibited a weaker activity compared with Pt/C catalysts, due to the exposure of nonactive Pd atoms on the surface. The Pd@Pt (21.2%) NWs exhibit the highest mass activity of 810 mA mg^{-1}_{Pt} (170 mA mg^{-1}_{Pt+Pd}) at 0.9 V vs RHE, which is 10 times greater than that of Pt/C catalyst versus Pt loading (2 times higher versus PtPd loading). The Pd@Pt NWs with atomic ratios of 21.2% and 28.5% have similar specific activity of ~0.4 mA cm^{-2}, 2-fold greater than that of Pt/C

DOI: 10.1021/jacs.5b03877
J. Am. Chem. Soc. 2015, 137, 7862−7868

catalysts (0.19 mA cm^{-2}). Xia et al. reported the synthesis and electrochemical performance of pure Pt nanoassemblies and ultrathin Pt NWs (self-supported electrode) exhibiting enhanced activity compared with Pt/C NPs.[25] Compared with the reported results, the present work proves that adding Pd atoms and forming a core−shell structure could enhance their activity to a large extent. The activity of Pd@Pt NWs increases in the following sequence: Pd@Pt NWs (6.0%) < Pd@Pt NWs (13.5%) < Pd@Pt NWs (21.2%) ≈ Pd@Pt NWs (28.5%), exhibiting the dependence on the Pt content and Pt shell thickness. For Pd@Pt (6.0%) and Pd@Pt (13.5%) NWs electrocatalysts, the Pt shell is thin enough (one to three monolayers) to produce ligand effects and strain effects.[5a,26] However, as shown in Figures 3 and 5, the Pt content is too low to cover the Pd NWs fully. For the Pd@Pt (21.2%) and Pd@Pt (28.5%) NWs electrocatalysts with a full coverage of Pt atoms deposited on Pd NWs, although the ligand effect is negligible, the strain effect dominates for the core−shell catalysts with less than five layers (estimated by the EDS line-scan analysis), explaining the excellent ORR activity.

The durability of the electrocatalysts was evaluated by cycling the potential between 0.5 and 1.1 V for 80k cycles in air-saturated 0.1 M $HClO_4$ solution at a sweep rate of 50 mV s^{-1} at room temperature. The changes of $E_{1/2}$, ECSA, mass activity, and specific activity for the Pd@Pt (21.2%) NWs and Pt/C catalysts are shown in Figure 7. Based on the CV measurements, the ECSA of Pd@Pt (21.2%) NWs had decayed by about 20% of its initial value, while the ECSA loss of Pt/C catalyst is 44% after 80k cycles (Figure 7C). However, the ECSA of Pd@Pt (21.2%) NWs increased during the first 40k cycles compared with its initial value, due to the removal of bromide ions on the NWs surface and thus exposure of more active sites. According to the EDS data shown in Table S2, the atomic ratio of bromide ions adsorbed on the catalysts decreased with increased potential cycling. For the Pt/C catalyst, there was an obvious negative shift in $E_{1/2}$ by 40 mV, the mass activity decreased to 24.3%, and the specific activity decreased to 42% of the initial data, respectively, after the stability tests. Conversely, Pd@Pt (21.2%) NWs exhibited the interesting result that the $E_{1/2}$ showed positive shifts of 13 mV and 11 mV after 60k and 80k potential cycles, respectively. The mass activity and specific activity increased to 195% (323 mA mg^{-1}_{Pt+Pd}) and 245% (0.98 mA cm^{-2}) of the initial values, respectively, after 60k cycles tests (Figure 7D). The variation of mass activity versus total metal loading is shown in Figure S10. With continued cycling, the activity starts to decrease but is still higher than the initial activity. The Pd@Pt (21.2%) NWs demonstrated improved durability in terms of resistance to loss of specific activity and mass activity. During stability tests, the bromide ions could be removed from the surface of the electrocatalysts during the potential cycling, updating and exposing more Pt active sites for oxygen adsorption and enhanced activity.[27] As shown in Figure S11A, the Pd@Pt (21.2%) NWs catalysts retained their ultrathin size and uniform 1D morphology after the stability tests. The formation of an inter-twined network structure of Pd@Pt (21.2%) NWs implies their excellent structure stability and membrane stability, which also play important roles for the excellent stability of Pd@Pt NWs.

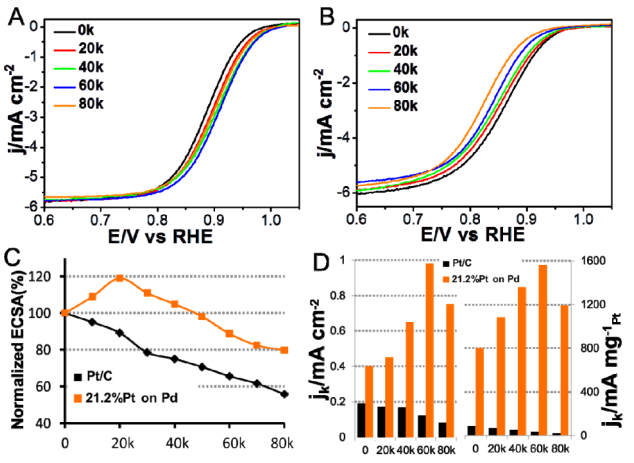

Figure 7. ORR polarization curves obtained in an oxygen-saturated 0.1 M $HClO_4$ solution at a sweep rate of 5 mV s^{-1} at 1600 rpm for the Pd@Pt (21.2%) NWs (A) and commercial Pt/C catalysts (B). (C) Specific ECSA for Pd@Pt (21.2%) NWs and Pt/C catalysts obtained prior to and following different potential cycles during durability testing. (D) Mass activity and specific activity shown as a function of durability cycling for the Pd@Pt (21.2%) NWs and Pt/C catalysts at 0.9 V (versus RHE).

CONCLUSIONS

In summary, we report a new route to prepare Pd@Pt core−shell NWs with controlled shell thickness triggered by bromide ions through a galvanic replacement reaction, which ensures its scalability. The bromide ions play an important role in initiating and promoting the reaction and then forming the core−shell NW structure. The uniform, smooth, and fully covered Pt shell is promoted by the Pt deposition process with slower kinetics. The Pd@Pt NWs are more active and durable than commercial Pt/C catalysts, due to their dominant (111) facets, smooth surface, Pd-induced compressive strain, and more corrosive Pt shell. The mass activity of Pd@Pt (21.2%) NWs is nearly 10 times greater than that of Pt/C catalysts versus Pt loading, which is strongly dependent on the Pt content and Pt shell thickness. Significant enhancements can be realized for the mass activity and specific activity for ORR through potential cycling. It has been found that the activity of Pd@Pt (21.2%) NWs increased after the durability tests, due to the removal of impurities and bromide ions from the surface to update and expose more active sites and superior structural stability to resolve the dilemma in using nanoparticles for alleviating the aggregation effect. This study provides a new design strategy for scalable preparation of novel heterogeneous 1D nanostructures with excellent activity and durability. Furthermore, the large-scale synthesized Pd@Pt NWs with controllable composition, shell thickness, and high aspect ratio may also provide a new platform for further engineering nanowire surfaces and compositions, or they may be used as building blocks for constructing 2D or 3D electrodes, and thus will have broad potential applications.

ASSOCIATED CONTENT

Supporting Information

TEM images of PdTe NWs, Pd core NWs, Pd@Pt NWs with different atomic ratios, and Pd@Pt (21.2%) NWs after stability tests; EDS analysis of the atomic ratio of bromide ions adsorbed on the catalysts; distribution of components in the Pd@Pt (6.0%), Pd@Pt (13.5%), and Pd@Pt (28.5%) NWs obtained by line-scan analysis using STEM-EDS; photographs of Pd NWs dispersion and the supernatants after centrifugation

DOI: 10.1021/jacs.5b03877
J. Am. Chem. Soc. 2015, 137, 7862−7868

of the products; ICP data of Pt^{2+} and Pd^{2+} in the supernatant solution after centrifugation of the products with different amount of KBr; CV profiles of Pd@Pt NWs with different atomic ratios. The Supporting Information is available free of charge on the ACS Publications website at DOI: 10.1021/jacs.5b03877.

AUTHOR INFORMATION

Corresponding Author

*shyu@ustc.edu.cn

Notes

The authors declare no competing financial interest.

ACKNOWLEDGMENTS

S.-H.Y. acknowledges funding support from the National Basic Research Program of China (Grants 2014CB931800, 2013CB933900), the National Natural Science Foundation of China (Grants 21407140, 21431006, 91227103), and Scientific Research Grant of Hefei Science Center of Chinese Academy of Sciences (Grant 2015SRG-HSC038). H.-H.L. is grateful to the China Postdoctoral Science Foundation (Grant 2014M560519).

REFERENCES

(1) (a) Debe, M. K. *Nature* **2012**, *486*, 43. (b) Cui, C. H.; Yu, S. H. *Acc. Chem. Res.* **2013**, *46*, 1427. (c) Chen, C.; Kang, Y.; Huo, Z.; Zhu, Z.; Huang, W.; Xin, H. L.; Snyder, J. D.; Li, D.; Herron, J. A.; Mavrikakis, M.; Chi, M.; More, K. L.; Li, Y.; Markovic, N. M.; Somorjai, G. A.; Yang, P.; Stamenkovic, V. R. *Science* **2014**, *343*, 1339. (d) Chen, G.; Zhao, Y.; Fu, G.; Duchesne, P. N.; Gu, L.; Zheng, Y.; Weng, X.; Chen, M.; Zhang, P.; Pao, C.-W.; Lee, J.-F.; Zheng, N. *Science* **2014**, *344*, 495. (e) van der Vliet, D. F.; Wang, C.; Tripkovic, D.; Strmcnik, D.; Zhang, X. F.; Debe, M. K.; Atanasoski, R. T.; Markovic, N. M.; Stamenkovic, V. R. *Nat. Mater.* **2012**, *11*, 1051. (f) Hernandez-Fernandez, P.; Masini, F.; McCarthy, D. N.; Strebel, C. E.; Friebel, D.; Deiana, D.; Malacrida, P.; Nierhoff, A.; Bodin, A.; Wise, A. M.; Nielsen, J. H.; Hansen, T. W.; Nilsson, A.; StephensIfan, E. L.; Chorkendorff, I. *Nat. Chem.* **2014**, *6*, 732.

(2) (a) Greeley, J.; Stephens, I. E. L.; Bondarenko, A. S.; Johansson, T. P.; Hansen, H. A.; Jaramillo, T. F.; RossmeislJ; ChorkendorffI; Nørskov, J. K. *Nat. Chem.* **2009**, *1*, 552. (b) Liang, H. W.; Cao, X.; Zhou, F.; Cui, C. H.; Zhang, W. J.; Yu, S. H. *Adv. Mater.* **2011**, *23*, 1467.

(3) (a) Liang, Y.; Li, Y.; Wang, H.; Dai, H. *J. Am. Chem. Soc.* **2013**, *135*, 2013. (b) You, H.; Yang, S.; Ding, B.; Yang, H. *Chem. Soc. Rev.* **2013**, *42*, 2880. (c) Zhou, Q.; Li, C. M.; Li, J.; Cui, X.; Gervasio, D. *J. Phys. Chem. C* **2007**, *111*, 11216. (d) Zhou, Q.; Li, C. M.; Li, J.; Lu, J. *J. Phys. Chem. C* **2008**, *112*, 18578.

(4) Yang, H. *Angew. Chem., Int. Ed.* **2011**, *50*, 2674.

(5) (a) Maark, T. A.; Peterson, A. A. *J. Phys. Chem. C* **2014**, *118*, 4275. (b) Wang, X.; Orikasa, Y.; Takesue, Y.; Inoue, H.; Nakamura, M.; Minato, T.; Hoshi, N.; Uchimoto, Y. *J. Am. Chem. Soc.* **2013**, *135*, 5938.

(6) Hsieh, Y. C.; Zhang, Y.; Su, D.; Volkov, V.; Si, R.; Wu, L.; Zhu, Y.; An, W.; Liu, P.; He, P.; Ye, S.; Adzic, R. R.; Wang, J. X. *Nat. Commun.* **2013**, *4*, 2466.

(7) (a) Sasaki, K.; Naohara, H.; Choi, Y.; Cai, Y.; Chen, W.-F.; Liu, P.; Adzic, R. R. *Nat. Commun.* **2012**, *3*, 1115. (b) Wang, D.; Xin, H. L.; Hovden, R.; Wang, H.; Yu, Y.; Muller, D. A.; DiSalvo, F. J.; Abruña, H. D. *Nat. Mater.* **2012**, *12*, 81. (c) Zhao, X.; Chen, S.; Fang, Z.; Ding, J.; Sang, W.; Wang, Y.; Zhao, J.; Peng, Z.; Zeng, J. *J. Am. Chem. Soc.* **2015**, *137*, 2804.

(8) (a) Gong, K.; Su, D.; Adzic, R. R. *J. Am. Chem. Soc.* **2010**, *132*, 14364. (b) Kuttiyiel, K. A.; Sasaki, K.; Choi, Y.; Su, D.; Liu, P.; Adzic, R. R. *Energy Environ. Sci.* **2012**, *5*, 5297. (c) Zhang, Y.; Hsieh, Y. C.; Volkov, V.; Su, D.; An, W.; Si, R.; Zhu, Y.; Liu, P.; Wang, J. X.; Adzic, R. R. *ACS Catal.* **2014**, *4*, 738.

(9) (a) Ferrando, R.; Jellinek, J.; Johnston, R. L. *Chem. Rev.* **2008**, *108*, 845. (b) Oh, A.; Baik, H.; Choi, D. S.; Cheon, J. Y.; Kim, B.; Kim, H.; Kwon, S. J.; Joo, S. H.; Jung, Y.; Lee, K. *ACS Nano* **2015**, *9*, 2856. (c) Zhang, S.; Hao, Y.; Su, D.; Doan-Nguyen, V. V. T.; Wu, Y.; Li, J.; Sun, S.; Murray, C. B. *J. Am. Chem. Soc.* **2014**, *136*, 15921.

(10) Zhu, H.; Zhang, S.; Su, D.; Jiang, G.; Sun, S. *Small* **2015**, DOI: 10.1002/smll.201500330.

(11) (a) Cao, K.; Zhu, Q.; Shan, B.; Chen, R. *Sci. Rep.* **2015**, *5*, 8470. (b) Feng, H.; Elam, J. W.; Libera, J. A.; Setthapun, W.; Stair, P. C. *Chem. Mater.* **2010**, *22*, 3133. (c) Hsu, I. J.; Hansgen, D. A.; McCandless, B. E.; Willis, B. G.; Chen, J. G. *J. Phys. Chem. C* **2011**, *115*, 3709.

(12) Park, J.; Zhang, L.; Choi, S. I.; Roling, L. T.; Lu, N.; Herron, J. A.; Xie, S.; Wang, J.; Kim, M. J.; Mavrikakis, M.; Xia, Y. *ACS Nano* **2015**, *9*, 2635.

(13) Guo, S.; Dong, S.; Wang, E. *Energy Environ. Sci.* **2010**, *3*, 1307.

(14) Cui, C.; Gan, L.; Heggen, M.; Rudi, S.; Strasser, P. *Nat. Mater.* **2013**, *12*, 765.

(15) Liang, H. W.; Guan, Q. F.; Chen, L. F.; Zhu, Z.; Zhang, W. J.; Yu, S. H. *Angew. Chem., Int. Ed.* **2012**, *51*, 5101.

(16) Wang, K.; Yang, Y.; Liang, H. W.; Liu, J. W.; Yu, S. H. *Mater. Horiz.* **2014**, *1*, 338.

(17) Li, H. H.; Zhao, S.; Gong, M.; Cui, C. H.; He, D.; Liang, H. W.; Wu, L.; Yu, S. H. *Angew. Chem., Int. Ed.* **2013**, *52*, 7472.

(18) Liang, H. W.; Liu, S.; Gong, J. Y.; Wang, S. B.; Wang, L.; Yu, S. H. *Adv. Mater.* **2009**, *21*, 1850.

(19) (a) Koenigsmann, C.; Zhou, W. P.; Adzic, R. R.; Sutter, E.; Wong, S. S. *Nano Lett.* **2010**, *10*, 2806. (b) Wang, J. X.; Inada, H.; Wu, L.; Zhu, Y.; Choi, Y.; Liu, P.; Zhou, W. P.; Adzic, R. R. *J. Am. Chem. Soc.* **2009**, *131*, 17298.

(20) (a) Kuttiyiel, K. A.; Sasaki, K.; Choi, Y.; Su, D.; Liu, P.; Adzic, R. R. *Energy Environ. Sci.* **2012**, *5*, 5297. (b) Strasser, P.; Koh, S.; Anniyev, T.; Greeley, J.; More, K.; Yu, C.; Liu, Z.; Kaya, S.; Nordlund, D.; Ogasawara, H.; Toney, M. F.; Nilsson, A. *Nat. Chem.* **2010**, *2*, 454.

(21) (a) Lim, B.; Jiang, M.; Tao, J.; Camargo, P. H. C.; Zhu, Y.; Xia, Y. *Adv. Funct. Mater.* **2009**, *19*, 189. (b) Xiong, Y.; Cai, H.; Wiley, B. J.; Wang, J.; Kim, M. J.; Xia, Y. *J. Am. Chem. Soc.* **2007**, *129*, 3665.

(22) Zhang, H.; Jin, M. S.; Wang, J. G.; Li, W. Y.; Camargo, P. H. C.; Kim, M. J.; Yang, D. R.; Xie, Z. X.; Xia, Y. N. *J. Am. Chem. Soc.* **2011**, *133*, 6078.

(23) Li, Y.; Wang, Z. W.; Chiu, C. Y.; Ruan, L.; Yang, W.; Yang, Y.; Palmer, R. E.; Huang, Y. *Nanoscale* **2012**, *4*, 845.

(24) (a) Xia, B. Y.; Wu, H. B.; Li, N.; Yan, Y.; Lou, X. W.; Wang, X. *Angew. Chem., Int. Ed.* **2015**, *54*, 3797. (b) Scofield, M. E.; Koenigsmann, C.; Wang, L.; Liu, H.; Wong, S. S. *Energy Environ. Sci.* **2015**, *8*, 350.

(25) (a) Xia, B. Y.; Wu, H. B.; Yan, Y.; Lou, X. W.; Wang, X. *J. Am. Chem. Soc.* **2013**, *135*, 9480. (b) Xia, B. Y.; Ng, W. T.; Wu, H. B.; Wang, X.; Lou, X. W. *Angew. Chem.* **2012**, *124*, 7325.

(26) Ding, X.; Yin, S.; An, K.; Luo, L.; Shi, N.; Qiang, Y.; Pasupathi, S.; Pollet, B. G.; Shen, P. K. *J. Mater. Chem. A* **2015**, *3*, 4462.

(27) Cai, Y.; Ma, C.; Zhu, Y.; Wang, J. X.; Adzic, R. R. *Langmuir* **2011**, *27*, 8540.

DOI: 10.1021/jacs.5b03877
J. Am. Chem. Soc. 2015, 137, 7862−7868